



### **Science Arts & Métiers (SAM)**

is an open access repository that collects the work of Arts et Métiers Institute of Technology researchers and makes it freely available over the web where possible.

This is an author-deposited version published in: <https://sam.ensam.eu>  
Handle ID: <http://hdl.handle.net/10985/21936>

#### **To cite this version :**

Enza PARENTE, Mirko FARANO, Pietro DE PALMA, Stefania CHERUBINI, Jean-Christophe ROBINET - Continuing invariant solutions towards the turbulent flow - Philosophical Transactions of the Royal Society A: Mathematical, Physical and Engineering Sciences - Vol. 380, p.20210031 - 2022

Any correspondence concerning this service should be sent to the repository

Administrator : [scienceouverte@ensam.eu](mailto:scienceouverte@ensam.eu)



# Continuing invariant solutions towards the turbulent flow

E. Parente<sup>1,2</sup>, M. Farano<sup>1,2</sup>, J.-Ch. Robinet<sup>2</sup>,

P. De Palma<sup>1</sup> and S. Cherubini<sup>1</sup>

<sup>1</sup>Department of Mechanics, Mathematics and Management,  
Politecnico di Bari, Via Re David 200, 70125 Bari, Italy

<sup>2</sup>Laboratoire DynFluid, Arts et Metiers ParisTech, Bd de l'Hopital  
75013 Paris, France

A new mathematical framework is proposed for characterizing the coherent motion of fluctuations around a mean turbulent channel flow. We search for statistically invariant coherent solutions of the unsteady Reynolds-averaged Navier–Stokes equations written in a perturbative form with respect to the turbulent mean flow, using a suitable approximation of the Reynolds stress tensor. This is achieved by setting up a continuation procedure of known solutions of the perturbative Navier–Stokes equations, based on the continuous increase of the turbulent eddy viscosity towards its turbulent value. The recovered solutions, being sustained only in the presence of the Reynolds stress tensor, are representative of the statistically coherent motion of turbulent flows. For small friction Reynolds number and/or domain size, the statistically invariant motion is almost identical to the corresponding invariant solution of the Navier–Stokes equations. Whereas, for sufficiently large friction number and/or domain size, it considerably departs from the starting invariant solution of the Navier–Stokes equations, presenting spatial structures, main wavelengths and scaling very close to those characterizing both large- and small-scale motion of turbulent channel flows.

This article is part of the theme issue ‘Mathematical problems in physical fluid dynamics (part 2)’.

## 1. Introduction

Understanding the dynamics of wall-bounded turbulent flows is a formidable challenge yet to be fully achieved, since turbulence is a complex phenomenon appearing in a variety of states and patterns which compete

with the laminar state [1]. In order to derive low-order models of the turbulent dynamics, one should focus on the coherent part of the turbulent motion [2], which is known to contribute much more to the momentum of the flow than the chaotic fluctuations at small scales. The most typical example of coherent motion in turbulent flows are the streaks, which have been first recognized by Kline *et al.* [3] as ‘surprisingly well-organized spatially and temporally dependent motions’. These elongated structures are continuously generated by the lift-up mechanism [4] within the self-sustained cycle theorized in the nineties [5,6]. Although this self-sustained process was initially observed in the inner layer region [5–7], a growing body of evidence has recently indicated that equivalent, mutually independent regeneration cycles are active in the logarithmic and outer regions as well [8–13], giving rise to large- and very-large-scale motion [14–18]. The statistical and dynamical features of these self-sustaining motions associated with streaks and quasi-streamwise vortices at different scales are consistent with Townsend’s attached eddy hypothesis [19]. Moreover, the same three fundamental mechanisms that compose the regeneration cycle of wall turbulence have been found to sustain several invariant solutions of the Navier–Stokes equations in the form of equilibria, travelling waves or (relative) periodic orbits [20–37], which compose the chaotic saddle sustaining transient turbulence [38]. Typical coherent structures populating transitional and turbulent flows, such as streaks and streamwise vortices, have been successfully captured by these fully nonlinear, dynamically unstable solutions of the Navier–Stokes equations which populate state space and support turbulent dynamics with their entangled stable and unstable manifolds. Trajectories in the state space may approach one of these solutions, remain in their neighbourhood for a finite time before being pushed away along one of the unstable directions to approach other solutions through heteroclinic orbits [39], resulting in a chaotic walk in the state space. Many efforts have been done for deriving low-order models based on these invariant solutions, allowing one to accurately describe the statistical properties of a turbulent flow [40]. Recently, Chandler & Kerswell [41] successfully applied the periodic orbit theory to the case of a two-dimensional Kolmogorov flow at a moderate Reynolds number. However, a low-order model of a fully developed three-dimensional turbulent flow is yet to be achieved, and would probably require the discovery of many new invariant solutions at sufficiently high Reynolds number. Unfortunately, the computation of such invariant solutions at large Reynolds number is a hard challenge, due to the multiple bifurcations they typically undergo. In the case of fully turbulent flows at high friction Reynolds number, a valuable approach for computing invariant solutions is resorting to large-eddy simulations (LES), as proposed by Hwang & Cossu [9,10]. In particular, choosing filtering widths larger than those typically used for reproducing results of direct numerical simulations (DNS), allows one to filter out a large range of scales that could not be resolved within the chosen numerical grid. This approach, relying on ‘overfiltered’ LES, with the Smagorinsky constant  $C_s$  controlling the strength of the filtering, is well suited for investigating the self-sustained nature of coherent large-scale motion, as done at first for the channel [9,10] and Couette [42,43] flows at relatively low Reynolds numbers and for the channel and asymptotic suction boundary layer flow at large friction Reynolds numbers [44,45]. Recent studies [9,10,43] have demonstrated that both large-scale and log-layer coherent motions can be self-sustained, since they survive in both channel and Couette flow, when smaller-scale active motions are artificially quenched and replaced by purely dissipative structures. However, this overfiltered approach does not allow one to investigate the nature of the energy transfer between coherent structures of different scales. Despite the motion at large scales can be sustained even when the wall cycle is quenched, in high-Reynolds-number turbulent flows multiple and non-trivial interactions exist between coherent structures at different scales [46,47]. Very recent works [48] have shown that wall-normal energy is transferred from large to small scales inducing energy production at the wall via the Orr mechanism, while a non-negligible amount of energy is transferred from small to large scales [47], possibly due to small-scale sinuous streak instability [48]. Thus, coherent structures at different scales are intimately connected by direct and inverse cascade mechanisms by which energy is transmitted scale-by-scale among different regions of the flow [46].

A deeper understanding of the energetic bond connecting small- and large-scale structure in turbulent flows can be achieved by the computation of statistically invariant coherent states which characterize the multiple-scale, coherent part of the motion around the turbulent mean flow, without any filtering of small-scale structures. Towards this aim, this work provides a new mathematical framework for the computation of statistically invariant equilibria, travelling waves or (relative) periodic orbits characterizing the motion of turbulent fluctuations around the mean flow. This is achieved by seeking for statistically invariant coherent solutions of the unsteady Reynolds-averaged Navier–Stokes equations written in a perturbative form with respect to the turbulent mean flow, using a suitable approximation of the Reynolds stress tensor. Unlike the classical invariant solutions of the Navier–Stokes equations, these solutions are sustained only in the presence of the Reynolds stress tensor, being representative of the statistically coherent motion of turbulence. This set of equations has been found efficient for characterizing extreme events having an energy spectrum very similar to that of the fully turbulent flow [49,50]. We show in this paper that, continuing in this statistical framework known invariant solutions of the Navier–Stokes equations at high friction Reynolds numbers, statistically invariant motions containing both large- and small-scale coherent structures such as streaks and streamwise vortices are obtained, with main wavelengths corresponding to the typical ones recovered in turbulent flows. The paper is structured as follows. In §2, the problem formulation is provided. In §3, the continuation procedure allowing the computation of the statistically invariant solutions is described. Relevant results are discussed in §4, and conclusions are drawn in §5.

## 2. Problem formulation

The incompressible flow in a channel is governed by the Navier–Stokes equations, which describe the dynamics of the instantaneous state variables  $\mathbf{q} = [\mathbf{u}, p]^T$ , where  $\mathbf{u}(\mathbf{x}, t)$  is the velocity field and  $p(\mathbf{x}, t)$  is the pressure.

When studying the flow dynamics in the vicinity of the laminar state, the state variables can be decomposed as the sum of the laminar base flow  $\mathbf{Q} = [U, 0, 0, P]^T$  and a perturbation  $\mathbf{q}' = [u', v', w', p']$ , leading to the Perturbative Navier–Stokes (PNS) equations

$$\text{and} \quad \left. \begin{aligned} \nabla \cdot \mathbf{u}' &= 0 \\ \frac{\partial \mathbf{u}'}{\partial t} &= -(\mathbf{u}' \cdot \nabla) \mathbf{u}' - (\mathbf{u}' \cdot \nabla) \mathbf{U} - (\mathbf{U} \cdot \nabla) \mathbf{u}' - \nabla p' + \frac{1}{Re} \nabla^2 \mathbf{u}', \end{aligned} \right\} \quad (2.1)$$

where  $Re = 3U_b/2(h/\nu)$  is the Reynolds number, defined on the basis of the bulk velocity  $U_b = \int_{-1}^1 U(y) dy$  (where  $3U_b/2$  corresponds to the value at the centreline of the parabolic laminar flow with mean velocity  $U_b$ ), the half channel height  $h$  and the kinematic viscosity  $\nu$ . Several invariant solutions of these equations, such as (relative) equilibria or periodic orbits, have been computed in the past decades [20–37].

Conversely, when studying the dynamics of coherent structures characterizing the turbulent flow, it can be appropriate to move the point of view in the vicinity of the turbulent mean flow. This is achieved by using a Reynolds decomposition approach similar to that used by Eitel-Amor *et al.* [51] and Farano *et al.* [49], where the flow vector is expressed as the sum of a mean flow  $\bar{\mathbf{Q}} = [\bar{\mathbf{U}}, P]^T = [\bar{\mathbf{U}}, 0, 0, \bar{P}]^T$  (where  $\bar{\bullet}$  denotes long-time and space averaging along the streamwise and spanwise directions) and a fluctuation  $\tilde{\mathbf{q}} = [\tilde{\mathbf{u}}, \tilde{p}]^T$ , comprising the coherent and incoherent part of the perturbations of the mean flow. Time- and space-averaging along the wall-parallel directions the Navier–Stokes equations, and subtracting these averaged equations from the Navier–Stokes equations leads to the perturbative Reynolds-averaged Navier–Stokes (PRANS) equations, which describe in a statistical way the nonlinear evolution of fluctuations of the mean turbulent flow as

$$\text{and} \quad \left. \begin{aligned} \nabla \cdot \tilde{\mathbf{u}} &= 0 \\ \frac{\partial \tilde{\mathbf{u}}}{\partial t} &= -(\tilde{\mathbf{u}} \cdot \nabla) \tilde{\mathbf{u}} - (\tilde{\mathbf{u}} \cdot \nabla) \bar{\mathbf{U}} - (\bar{\mathbf{U}} \cdot \nabla) \tilde{\mathbf{u}} - \nabla \tilde{p} + \frac{1}{Re} \nabla^2 \tilde{\mathbf{u}} + \nabla \cdot \overline{\tilde{\mathbf{u}} \tilde{\mathbf{u}}}, \end{aligned} \right\} \quad (2.2)$$

where the term  $\overline{\mathbf{u}\mathbf{u}}$  is the Reynolds stress tensor  $\tau$ . Note that steady solutions of the PRANS equations, as well as the mean flow itself, are sustained by the Reynolds stress term, which is in turn sustained by the coherent and incoherent part of the fluctuations. The mean velocity profile for channel flow is well approximated by the analytical expression proposed by Reynolds & Tiedermann [52]

$$\frac{d\overline{U}^+}{dy} = -\frac{Re_\tau y}{v_T^+(y)}, \quad (2.3)$$

$Re_\tau = u_\tau h/\nu$  being the friction Reynolds number based on the friction velocity  $u_\tau = \sqrt{\tau_w/\rho}$ , where  $\tau_w$  is the wall shear stress, and  $v_T^+ = v_T/\nu$  is the ratio between the total viscosity  $v_T = \nu + \nu_t$  and the kinematic viscosity  $\nu$ ,  $\nu_t$  being the turbulent eddy viscosity. The total eddy viscosity is modelled using Cess analytic approximation [53], as assumed in previous works [54–56]. Since this mean velocity profile is not solution of the Navier–Stokes equations, in order to close the problem, the divergence of the Reynolds stress tensor  $\tau$  in equation (2.2) needs to be modelled. A common way to write this term is using the Boussinesq’s Eddy Viscosity hypothesis  $\tau_{ij} = -\tilde{u}_i \tilde{u}_j = \nu_t \bar{S}_{ij}$  [57], where  $\bar{S}$  is the shear stress tensor. Considering a fully developed channel flow whose statistics are averaged in the streamwise and spanwise direction, the divergence of the Reynolds stress tensor has only two non-zero components, i.e.  $d\tau_{12}(y)/dy$  and  $d\tau_{22}(y)/dy$  (note that the latter term cannot be incorporated in the pressure term since the other isotropic components have derivative equal to zero). The former term is approximated using the above mentioned eddy viscosity hypothesis, while the latter is modelled by using the rescaling proposed by Chen *et al.* [58], as

$$\overline{u\tilde{u}} = -\nu_t \frac{d\overline{U}}{dy} \quad \text{and} \quad \overline{v\tilde{v}}^+ = \overline{u\tilde{u}}^+ \left( \frac{l_{22}^+}{l_{12}^+} \right)^2, \quad (2.4)$$

$l_{12}^+, l_{22}^+$  being the Reynolds stress lengths defined as

$$l_{i2}^+ = c_{i2} y^{+(i+2)/2} \left( 1 + \left( \frac{y^+}{y_{\text{sub}}^+} \right)^4 \right)^{1/8} \left( 1 + \left( \frac{y^+}{y_{\text{buf}}^+} \right)^4 \right)^{-(1+i)/4} \frac{1 - r^4}{4(1 - r)} \left( 1 + \left( \frac{r_{\text{core}i2}}{r} \right)^2 \right)^{i/4}, \quad (2.5)$$

where  $i = 1, 2$ ,  $r = 1 - y$  is the distance from the centreline,  $y_{\text{sub}}^+ = 9.7$  is the sublayer thickness,  $y_{\text{buf}}^+ = 41$  is the buffer layer thickness,  $r_{\text{core}12} = 0.27$  and  $r_{\text{core}22} = 0.3$  are the central core layers, and the parameters  $c_{12}, c_{22}$  are function of these quantities (see [58] for further details). This analytical formulation has been validated by comparing the mean turbulent flow and the Reynolds stress tensor components with those obtained by DNS at  $Re = 3300$  ( $Re_\tau = 180$ ) [59] and at  $Re = 12450$  ( $Re_\tau = 590$ ) [60]. The results obtained are computed in this range of Reynolds numbers, for which turbulence is fully developed (not spatially patterned) and both the mean flow and the Reynolds stress are accurately described by the chosen analytical approximation.

### 3. Continuation from the PNS to the PRANS framework

Statistically invariant travelling waves solutions of the PRANS equations are sought for by continuation of known invariant solutions of the PNS equations. In particular, as sketched in figure 1, a homotopy procedure is used for continuously passing from equations (2.1) to (2.2), which have an almost identical structure, except for the steady flow used as reference and for the presence of the Reynolds stress tensor. Since these quantities depend directly on the turbulent eddy viscosity, the continuation is performed by continuously increasing this quantity from zero to its characteristic turbulent value expressed by the Cess model [53]. Towards this purpose, we define an effective turbulent eddy viscosity,  $\epsilon \nu_t$ , where  $\epsilon$  is a real positive number in the range  $[0, 1]$ , and  $\nu_t$  is expressed as

$$\nu_t = \frac{\nu}{2} \left\{ 1 + \left( \frac{\kappa^2 Re_\tau^2}{9} \right) (2\hat{\eta} - \hat{\eta}^2)^2 (3 - 4\hat{\eta} + 2\hat{\eta}^2)^2 \left\{ 1 - \exp \left[ \frac{(|\hat{\eta} - 1| - 1) Re_\tau}{A} \right] \right\}^2 \right\}^{\frac{1}{2}} - \frac{1}{2}. \quad (3.1)$$

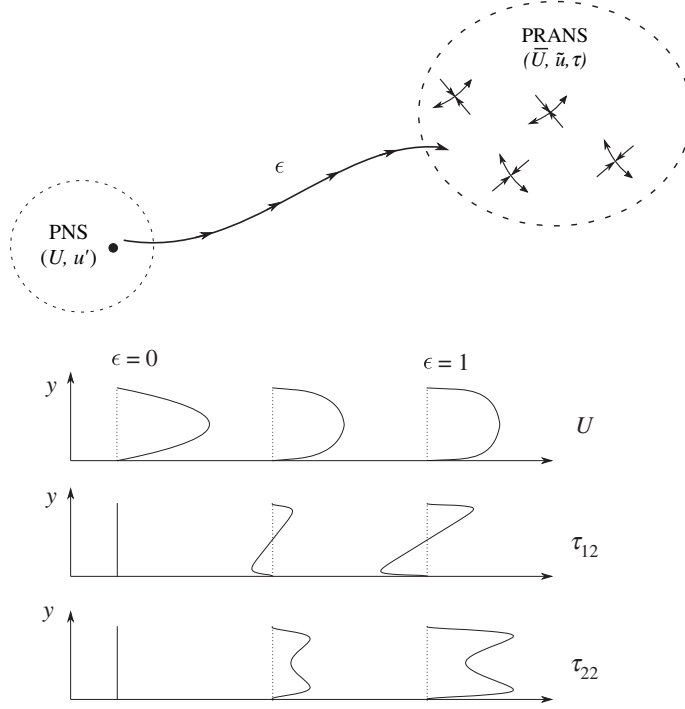


**Figure 1.** Schematic visualization of the continuation procedure from the Perturbative Navier–Stokes equations ( $\epsilon = 0$ ) to the Perturbative Unsteady Reynolds-averaged Navier–Stokes equations ( $\epsilon = 1$ ).

with  $\hat{\eta} = \eta + 1$  defined in the domain  $[0, 2]$ ,  $\kappa = 0.426$  and  $A = 25.4$ , as assumed in previous works [55,56,61]. Continuation from the PNS to the PRANS equations is achieved by increasing the coefficient  $\epsilon$  from 0 to 1, and using the effective turbulent eddy viscosity  $\epsilon \nu_t$  in the analytical expression of the Reynolds stress tensor components  $\tau_{11}, \tau_{12}$  in equation (2.4) and in the mean flow profile in equation (2.3), where  $\nu_t^+ = 1 + \epsilon \nu_t / \nu$ . The procedure consists in selecting a known travelling wave solution of the Navier–Stokes equations, subtracting the laminar flow solution for defining the corresponding perturbation, which is a travelling wave solution of equations (2.1), and continuing it in  $\epsilon$  using the following equations:

$$\left. \begin{aligned} \nabla \cdot \tilde{\mathbf{u}} &= 0 \\ -C \frac{\partial \tilde{\mathbf{u}}}{\partial x} &= -(\tilde{\mathbf{u}} \cdot \nabla) \tilde{\mathbf{u}} - (\tilde{\mathbf{u}} \cdot \nabla) \bar{\mathbf{U}} - (\bar{\mathbf{U}} \cdot \nabla) \tilde{\mathbf{u}} - \tilde{\nabla} p + \frac{1}{Re} \nabla^2 \tilde{\mathbf{u}} - \nabla \cdot \epsilon \nu_t \bar{\mathbf{S}}(\bar{\mathbf{U}}) \\ \bar{\mathbf{U}}(y) &= \left[ 1 - \int \frac{Re_\tau^2 y}{Re(1 + \epsilon(\nu_t/\nu))} dy, 0, 0 \right]^T, \end{aligned} \right\} \quad (3.2)$$

where  $C$  is the phase velocity of the Galilean frame in which the solution is steady.

When  $\epsilon = 0$ ,  $Re_\tau^2 = 2Re$  and one recovers  $\bar{\mathbf{U}} = 1 - y^2 = U$ , the Reynolds stress tensor components being null. In this limit, equations (3.2) coincide with the PNS equations (2.1) and consequently  $\tilde{\mathbf{u}}$  coincides with  $u'$ . When  $\epsilon = 1$ , one gets the turbulent expression of  $\nu_t$  given in equation (3.1), so that the turbulent mean velocity profile and the Reynolds stress tensor components in equations (2.4) are obtained. Note that, similarly to a homotopy procedure, the solutions obtained for  $\epsilon \in ]0, 1[$  have no physical sense. Moreover, for  $\epsilon \neq 1$ ,  $\tilde{\mathbf{u}}$  can have a non-zero mean, since  $\bar{\mathbf{U}}$  represents the mean flow only in turbulent conditions, which are achieved only for  $\epsilon = 1$ . The whole procedure, which is sketched in figure 1, is implemented within the open-source software Channelflow ([channelflow.ch](http://channelflow.ch)) [62].

Continuation from the PNS to the PRANS equations is performed enforcing a constant volume flux and consequently fixing the bulk velocity. Thus, while  $\epsilon$  increases from 0 to 1, the friction Reynolds number grows from the laminar ( $Re_\tau^L$ ) towards the turbulent ( $Re_\tau^T$ ) value as

$$Re_\tau = (1 - \epsilon)Re_\tau^L + \epsilon Re_\tau^T = [(1 - \epsilon)u_\tau^L + \epsilon u_\tau^T] \frac{h}{\nu}, \quad (3.3)$$

where  $u_\tau^L = \sqrt{3U_b\nu/h}$  is the friction velocity of the laminar flow and  $u_\tau^T$  is the friction velocity of the turbulent flow, which, using Dean's approximation for the skin friction in fully turbulent flow [63], can be expressed as

$$u_\tau^T = \sqrt{\frac{0.073}{2}} U_b^2 \left( \frac{2U_b h}{\nu} \right)^{-0.025}. \quad (3.4)$$

## 4. Results

As a first attempt aiming at validating the approach, we take as a starting point for the continuation procedure the travelling wave solution *TW2* obtained by Gibson & Brandt [33] in a small domain at low Reynolds number. This invariant solution of the NS equations is computed at  $Re = 2300$  in a domain of extension  $2\pi \times 2 \times \pi$ , with  $32 \times 97 \times 64$  points in the streamwise ( $x$ ), wall-normal ( $y$ ) and spanwise ( $z$ ) direction, respectively. As shown in figure 2a, the *TW2* solution is continued with respect to the Reynolds number up to  $Re = 3800$ , which is sufficiently high for displaying featureless (not patterned) turbulence. As shown in figure 3a, the *TW2* solution at this value of  $Re$  consists of two layers of counter-rotating vortices and slightly modulated streaks along the lower wall, and one layer of counter-rotating vortices along the upper wall (not shown). This solution is continued to the PRANS formulation by increasing the eddy viscosity as explained in section (3). Continuation is performed at fixed Reynolds number  $Re = 3800$ , enforcing a constant volume flux. The variation of the streamwise velocity norm during this continuation procedure is shown in figure 2b. After an initial drop, the streamwise velocity norm increases with  $\epsilon$ , reaching for  $\epsilon = 1$  a value about 60% larger with respect to its initial value. Moreover, when  $\epsilon = 1$ , the friction Reynolds number reaches  $Re_\tau = 134.521$ , and the statistically invariant solution *TW2<sub>T</sub>*, shown in figure 3b, is obtained. Note that this friction Reynolds number is rather low for a fully developed turbulent flow, we thus expect the solution to slightly change when continued towards the PRANS framework. Comparing this statistically steady solution with the starting travelling wave, one can observe that the quasi-streamwise vortices (blue and red isosurfaces) are almost unchanged, while strong differences can be noticed on the velocity streaks, which are less fragmented, more streamwise-aligned and shifted towards the wall. This shift of the streaks towards the wall can presumably be due to the wall-normal variation of the eddy viscosity used in the PRANS equations. As discussed in [56], since in the near-wall region and lower part of the logarithmic region, the eddy viscosity grows linearly with  $y$ , coherent structures are allowed to reach larger amplitudes, so they protrude towards the wall. Whereas, they weaken in the upper part of the logarithmic region and outer region, due to the large value of  $\nu_t$ . Moreover, the streaks considerably increase their size in the spanwise direction, and show a peculiar triangular shape. This peculiar shape compares very well with the streaky mean flow obtained by optimally forcing a turbulent channel flow, while the vortical structures remember closely the most energetic DMD mode recovered on top of this streaky flow [64]. The streaks reach down towards the wall, where they are almost streamwise aligned, while they present some wiggles close to the streamwise vortices. Moreover, their structures becomes almost identical on the two walls, despite in the upper wall much weaker vortices are found (not shown).

These unexpected differences with respect to the starting *TW2* solution might arise from the fact that, when continuing the PNS equations (2.1) towards the PRANS ones (2.2), invariant perturbations of the laminar base flow transform into statistically coherent fluctuations of the mean flow. Thus, the observed structural change of the travelling wave solution can be simply due to the change of reference from the base to the mean flow, rather than to an intrinsic modification of the coherent motion. An answer to this important point can be found by directly comparing



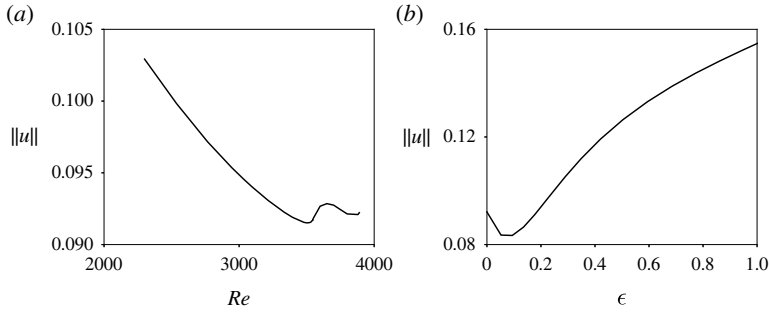


**Figure 2.** Continuation diagram of the streamwise velocity norm of  $TW2$  with respect to  $Re$  (a) for  $\epsilon = 0$ , and with respect to  $\epsilon$  for  $Re = 3800$  (b).

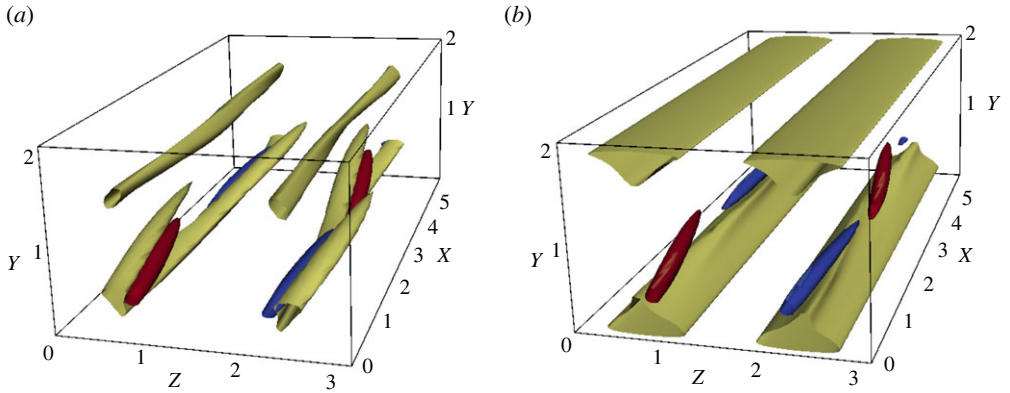


**Figure 3.** Invariant  $TW2$  solution for  $\epsilon = 0$  (a) and  $\epsilon = 1$  (b) for  $Re = 3800$ : isosurfaces of negative streamwise velocity ((a)  $u' = -0.11$ , (b)  $\tilde{u} = -0.15$ , light grey in the printed version, yellow online) and  $Q$ -criterion ( $Q = 0.1$ ) coloured by the streamwise vorticity (dark grey in the printed version; red for positive, blue for negative online). (a)  $\epsilon = 0$ , (b)  $\epsilon = 1$ . (Online version in colour.)

the instantaneous flow fields of  $TW2$  and  $TW2_T$ , obtained by summing up the perturbations (fluctuations) provided in the left (right) frame of figure 3 to the base (mean) flow, respectively. The difference between these two flow field is found to be of  $\mathcal{O}(10^{-4})$ , three orders of magnitude smaller than the perturbation maximum amplitude, thus validating our procedure at such a low friction Reynolds, for which the dynamics of fluctuations of the mean flow should not strongly differ to that of perturbations of the base flow after a mere change of reference.

Once our approach has been validated, we attempt to increase the friction Reynolds number for reaching values typical of fully turbulent flows. First, we tried to continue the  $TW2_T$  solution further in  $Re$ , but the convergence of higher- $Re$  solutions was very slow and time-consuming. Conjecturing that the domain might be too small for capturing statistically steady coherent structures typical of higher-Reynolds number flows, we have continued  $TW2_T$  in the streamwise direction up to  $L_x = 9.54$ , while keeping  $U_b$  fixed. This solution, provided in figure 4a, is very similar to that previously shown, showing coherent, large-scale streaks with smaller vortices on top of them. One can again note the strong similarity of this solution with the main energetic structures found in a forced DNS of turbulent channel flow [64]. However, this solution is again characterized by a rather low  $Re_\tau = 134.5$ , thus the difference between the relative instantaneous flow fields, shown in figure 4b, is again very small. This  $TW$  is then continued in Reynolds number up to  $Re = 5945$ , corresponding to  $Re_\tau = 199.0$ , which is only slightly higher than that



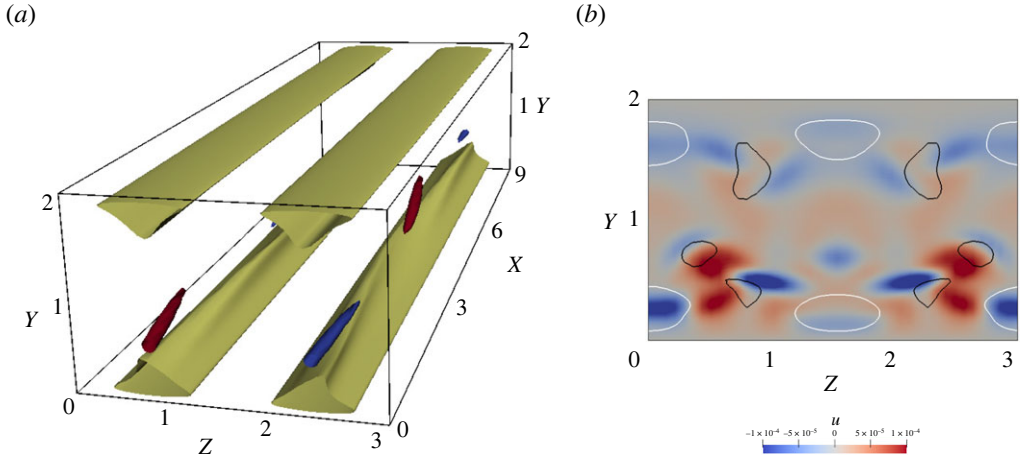


**Figure 4.** (a) Statistically steady travelling wave solution  $TW2_T$ , for  $Re = 3800$  and  $L_x = 9.544$ : isosurfaces of negative streamwise velocity ( $\tilde{u} = -0.15$ , light grey in the printed version, yellow online) and Q-criterion ( $Q = 0.08$ ) coloured by the streamwise vorticity (dark grey in the printed version, red for positive, blue for negative online). (b) Difference of the instantaneous flow fields of  $TW2$  and  $TW2_T$  (shaded contours) and streamwise velocity perturbation associated with the travelling wave solution  $TW2$  (black line for negative, white line for positive) for  $Re = 3800$  and  $L_x = 9.544$ . (a)  $\tilde{u}$ , (b)  $u_{TW2_T} - u_{TW2}$ . (Online version in colour.)

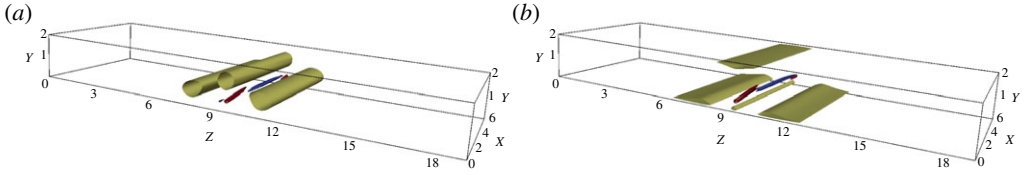


**Figure 5.** Travelling wave solution  $TW2 - 1$  for  $\epsilon = 0$  (a) and  $\epsilon = 1$  (b) for  $Re = 3300$  and  $U_b = 1$ : isosurfaces of negative streamwise velocity (light grey in the printed version, yellow online for (a)  $u' = -0.25$ , (b)  $\tilde{u} = -0.46$ ) and Q-criterion ( $Q = 0.1$ ) coloured by the streamwise vorticity (dark grey in the printed version, red for positive, blue for negative online). (a)  $\epsilon = 0$ ,  $Re_\tau = 99.5$ , (b)  $\epsilon = 1$ ,  $Re_\tau = 210.0$ . (Online version in colour.)

characterizing the  $TW2_T$  solution at  $Re = 3800$ . Further continuation of this invariant solution of the PRANS equation with respect to  $Re$  was again very slow and time-consuming.

Motivated by these results, we have chosen a new starting point of the continuation procedure, namely, a spanwise-localized travelling wave solution called  $TW2 - 1$  [33], whose similarity to flow structures characterizing the near-wall cycle has been reported in the literature. This travelling wave solution, which has been obtained by continuation of  $TW2$  after windowing on a larger spanwise domain [33], is similar in structure to  $TW2$ , although being mostly concentrated towards one wall. We have first obtained the  $TW2 - 1$  solution at  $Re = 3300$  in the domain of size  $2\pi \times 2 \times 6\pi$ , with  $32 \times 97 \times 324$  points in the streamwise, wall-normal and spanwise direction, respectively. The  $TW2 - 1$  solution is continued at first with respect to the bulk velocity, in order to increase its friction Reynolds number. The resulting travelling wave is shown in figure 5a for  $Re = 3300$ . This spanwise-localized solution consists of slightly modulated streaks flanked by streamwise-inclined vortices, which are weaker on the upper wall, where only one streaks pair is observed, and stronger on the bottom wall, where two pairs of streaks are recovered.

This  $TW2 - 1$  solution is then continued to the PRANS equations varying the parameter  $\epsilon$  from 0 to 1, at fixed  $Re = 3300$  and  $U_b$ . Figure 5b provides this solution at  $Re = 3300$ , corresponding to  $Re_\tau = 210$ . The lateral streaks on the bottom wall and that on the upper wall considerably increase

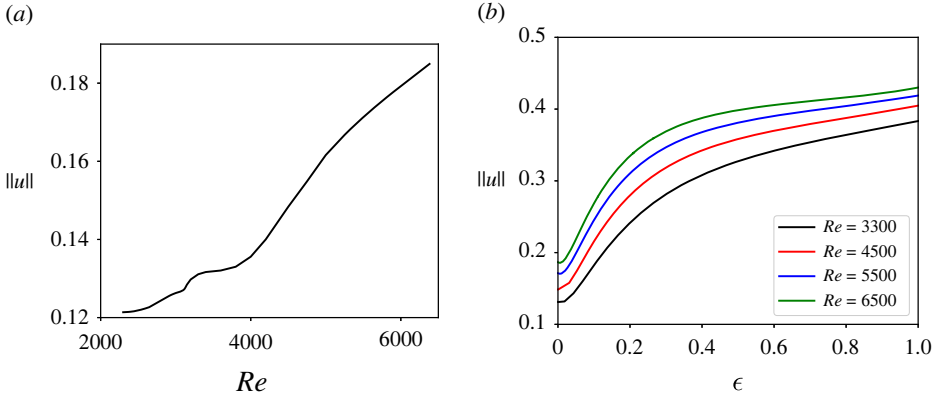


**Figure 6.** Continuation diagram for the travelling wave solution  $TW2 - 1$  versus  $Re$  for  $U_{\text{bulk}} = 1$ : norm of the streamwise velocity (a) and of the wall-normal velocity (b). (Online version in colour.)

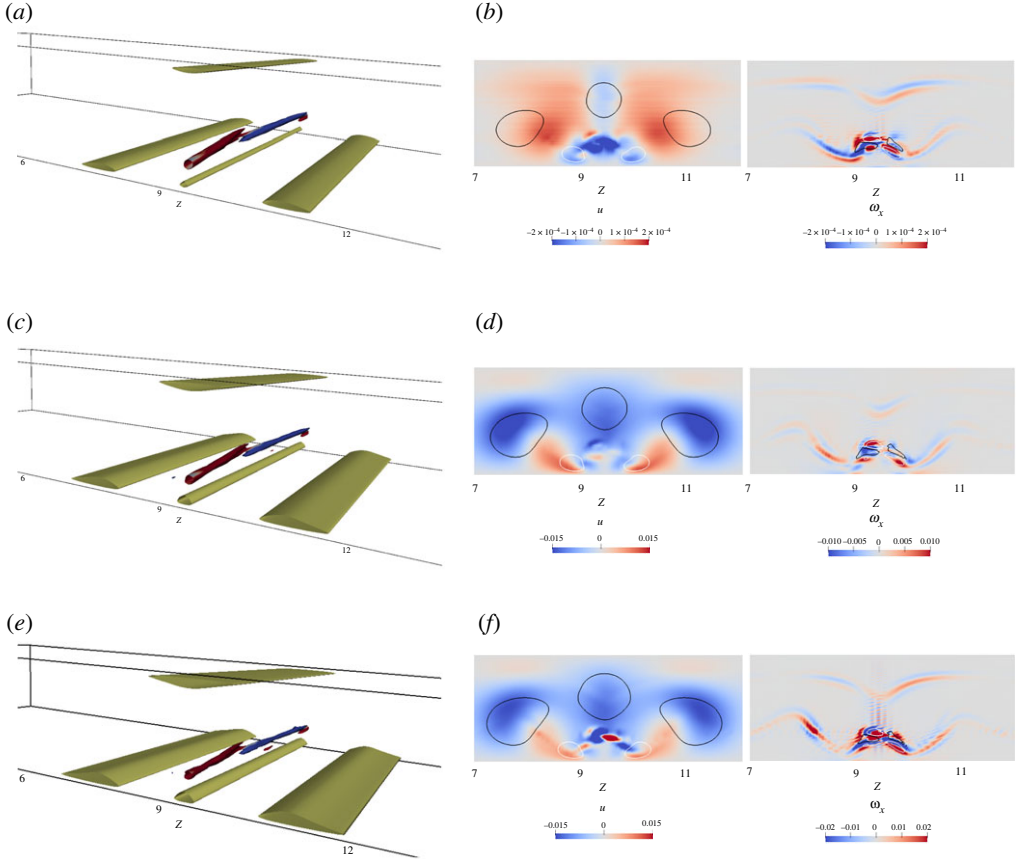


**Figure 7.** (a,c,e) Travelling wave solution  $TW2 - 1_f$  at different Reynolds numbers: isosurfaces of negative streamwise velocity ( $\tilde{u} = -0.55$ , light grey in the printed version, yellow online) and Q-criterion ( $Q = 0.1$ ) coloured by the streamwise vorticity (dark grey in the printed version, red for positive, blue for negative online). (b,d,f) Solid velocity and vorticity contours associated with the travelling wave solution  $TW2 - 1$  obtained with  $\epsilon = 0$  (black line for negative, white line for positive), and difference between the two instantaneous solutions  $u_{TW2-1_f} - u_{TW2-1}$  (shaded contours for the streamwise velocity and vorticity, see legend). (a)  $Re = 4500$ ,  $\tilde{u}$ , (b)  $Re = 4500$ ,  $u_{TW2-1_f} - u_{TW2-1}$ , (c)  $Re = 5500$ ,  $\tilde{u}$ , (d)  $Re = 5500$ ,  $u_{TW2-1_f} - u_{TW2-1}$ , (e)  $Re = 6500$ ,  $\tilde{u}$ , (f)  $Re = 6500$ ,  $u_{TW2-1_f} - u_{TW2-1}$ . (Online version in colour.)

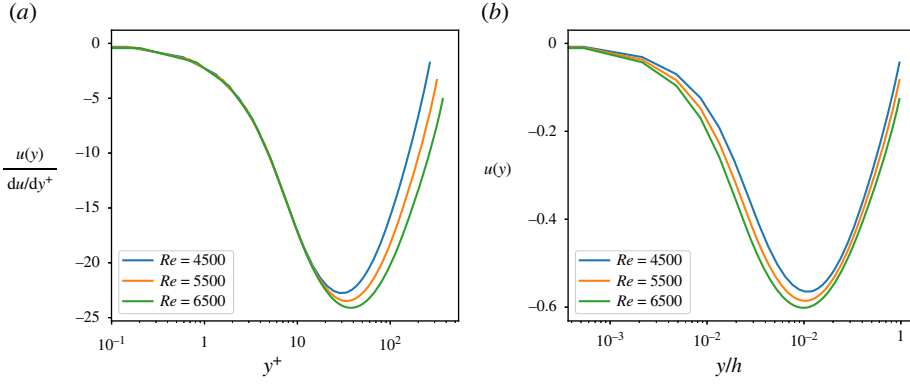


**Figure 8.** Streamwise-averaged velocity profile of the  $TW2 - 1_7$  extracted at the  $z$  location where the central small-scale streak presents its maximum value, scaled in inner (a) and outer (b) units. (Online version in colour.)

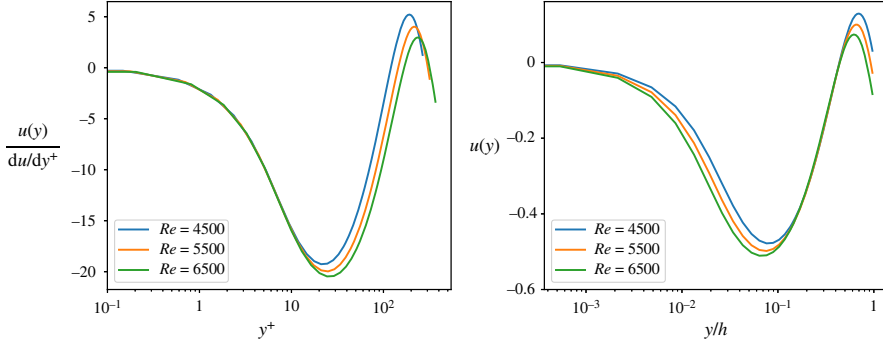


**Figure 9.** Streamwise-averaged velocity profile of the  $TW2 - 1_7$  extracted at the  $z$  location where the lateral large-scale streaks present their maximum value, scaled in inner and outer units. (Online version in colour.)

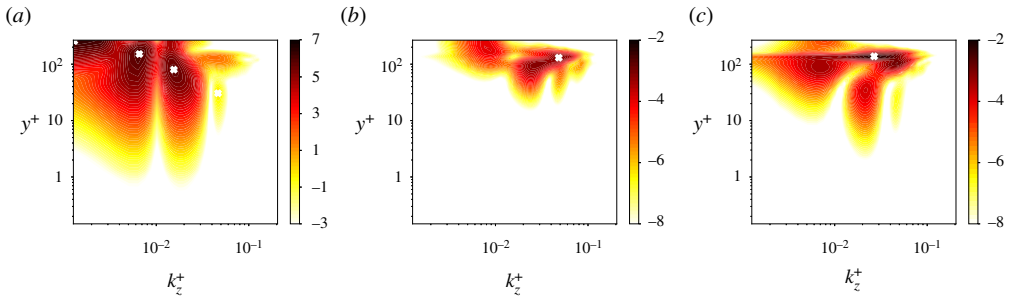


**Figure 10.** Premultiplied one-dimensional spanwise spectra of the streamwise (a), wall-normal (b) and spanwise velocity (c) of  $TW2 - 1_7$  at  $Re = 4500$ . (a)  $k_z E_{uu}(k_z)$ , (b)  $k_z E_{vv}(k_z)$ , (c)  $k_z E_{ww}(k_z)$ . (Online version in colour.)

their size in the spanwise direction, reaching a width which appears to be close to that typical of large-scale motion,  $\lambda_z \approx 1.5h$  [65]. For reaching higher values of  $Re_\tau$ , continuation with respect to  $Re$  of  $TW2 - 1$  is performed, keeping  $U_b$  fixed. The variation of the norm of the streamwise velocity of  $TW2 - 1$  during the  $Re$ -continuation is found in figure 6a, showing a continuous increase of this quantity, while the wall-normal velocity considerably decreases with  $Re$  (not shown). Several solutions at increasing values of  $Re$  have been then continued in  $\epsilon$  towards

the PRANS framework, as shown in figure 6b. Figure 7a,c,e provides the  $TW2 - 1_T$  solutions at different values of the Reynolds number up to 6500 (corresponding to  $Re_\tau = 380.03$ ). The whole structure of the travelling wave remains similar to that recovered at  $Re = 3300$ , although the streaks become stronger while the counter-rotating vortices slightly weaken. More importantly, as shown in figure 7b,d,f, the difference between the instantaneous flow fields of the corresponding TW solutions of the PNS and PRANS equations consistently increases, now reaching the same order of magnitude of the perturbation itself. This means that the structural modifications of  $TW2 - 1_T$  with respect to  $TW2 - 1$  at high  $Re_\tau$ , do not depend only on the change of reference from the laminar base flow to the mean turbulent flow, but to an intrinsic difference in the coherent disturbances dynamics. Figure 7b,d,f shows a cross-section of the low- and high-speed streaks of  $TW2-1$  (black and white lines) at different Reynolds numbers, together with the difference between the instantaneous flow fields of  $TW2 - 1$  and  $TW2 - 1_T$  at the same values of  $Re$  (shaded contours). One can note that the largest modifications are observed on the lateral low-speed streaks, which increase their spanwise size and move towards the wall, and on the high-speed ones at the wall, which appear to be change their spanwise size too (not shown). However, while the streamwise velocity is modified in a large part of the domain, the counter-rotating vortices change exclusively in a very narrow zone between the low- and high-speed streaks. The result of these modification is a consistent increase of the spanwise size of most of the streaks, which reach a length comparable to the channel half-height, typical of large scale motion [11,17,65]. A smaller-size streak is observed as well, having spanwise size  $\mathcal{O}(100)$  (in inner units), close to that typical of wall streaks. However, this smaller-scale coherent structure does not appear directly linked to the wall cycle, since, as shown in figure 8a, its streamwise-averaged velocity profile extracted at  $z = 9$  and scaled with respect to the inner units, appears not to be independent of  $Re_\tau$ , as one would expect for wall-cycle related structures. In particular, its peak scales approximately with  $Re_\tau^{1/2}$ , as one would expect for large-scale structures [56]. It is worth to note that the same scaling with respect to  $Re_\tau$  characterizes the lateral large-scale streaks, whose inner-scaled velocity profiles are shown in figure 9a. However, comparing figures 8b and 9b, one can also note that, while the lateral streaks present a robust outer scaling, confirming their large-scale nature, for the small-scale central streak the velocity profiles at different  $Re_\tau$  do not collapse at large values of  $y$ . Thus, the small-scale central streak cannot directly be related with the wall cycle, but neither to the large-scale structures, probably being linked to the secondary motion induced by the vortical structures placed at the centre of the domain. These counter rotating vortices placed in the region between the large-scale streaks, reaching much higher distances from the wall, remember the typical vortical structures recovered in large-scale motion (also called bulges).

A quantitative analysis of the main spanwise wavelengths of  $TW2 - 1_T$  has been carried out by computing the premultiplied energy spectra of the streamwise, wall-normal and spanwise velocities of this solution at  $Re = 4500$  (corresponding to  $Re_\tau = 275.47$ ), which are shown in figure 10a,b,c, respectively. Concerning the streamwise velocity, the lowest-wavenumber peak ( $k_z^+ = 0.00127$  or  $k_z = 0.35$  in outer units) corresponds to the size of the TW envelope, being close to the spanwise domain size. Two other peaks are recovered for  $k_z^+ = 0.0065$  and  $k_z^+ = 0.0155$ , corresponding to wavelengths  $\lambda_z = 3.5$  and  $\lambda_z = 1.47$  in outer units, respectively, lying in the range of the typical spanwise size of large-scale motion (reported to be  $\lambda_z = 1 - 3$  in outer units). A higher-frequency, weaker peak is found for  $k_z^+ = 0.047$ , corresponding to  $\lambda_z^+ = 135$ , which is rather close to the typical spanwise size of wall-streaks. Whereas, the wall-normal and spanwise spectra are both characterized by one peak only, at  $k_z^+ = 0.048$  (corresponding to  $\lambda_z^+ = 130.08$ ) and  $k_z^+ = 0.026$  ( $\lambda_z^+ = 235.32$ ), respectively. Notice that these wavelengths are much lower than the dominant ones of the streamwise velocity spectra, being closer to those typical of the wall cycle. Very similar spectra are recovered at  $Re = 5500$  and  $Re = 6500$  (corresponding to  $Re_\tau = 328.35$  and  $Re_\tau = 380.03$ , respectively), indicating that the structure of  $TW2 - 1_T$  remains robust when the Reynolds number increases. Moreover, it is interesting to evaluate the scaling of the relevant structures of these solutions with respect to those of the single self-sustaining attached eddy [11], which is composed of a long streaky motion reaching the near-wall region, self-similar along  $y = 0.1\lambda_z$  and a shorter vortical structure carrying all the velocity components, self-similar along

$y = 0.5 - 0.7\lambda_z$ . A very similar scaling is found in the  $TW2 - 1_T$  solution, with the two dominant peaks in the streamwise velocity spectrum having  $y \approx 0.1 - 0.15\lambda_z$  while a scaling of  $y \approx 0.58\lambda_z$ ,  $y \approx \lambda_z$  is found in the spanwise and wall-normal spectra, respectively. The statistically steady solution presented here, composed of large streaky structures and short vortical ones carrying all velocity components, is thus similar in shape and wavelengths to the self-sustaining structures of the attached eddy theory [11]. However, in this solution, large- and small-scale structures are not torn apart, but tied together in a non-trivial way, representing one potential first brick for the development of a low-order model of turbulence dynamics.

## 5. Conclusion

In this work, we propose a new mathematical framework for characterizing the coherent motion of turbulent fluctuations around the mean flow in a turbulent channel, using a statistical point of view. In particular, we search for statistically invariant coherent solutions of the unsteady Reynolds-averaged Navier–Stokes equations written in a perturbative form with respect to the turbulent mean flow, using a suitable approximation of the Reynolds stress tensor. For doing so, we set up a continuation procedure of known invariant solutions of the perturbative Navier–Stokes equations, based on the continuous increase of the eddy viscosity towards its turbulent value. The recovered solutions are sustained only in the presence of the Reynolds stress, thus being representative of the coherent motion of turbulent flows. The travelling wave  $TW2$  has been first used as a starting point of the continuation procedure, and continued to the turbulent framework up to friction Reynolds number  $Re_\tau \approx 134.52$ . Although structural changes are found in the solution, when resorting to instantaneous quantities the statistically invariant motion results to be only marginally different to the corresponding invariant solution of the Navier–Stokes equations. This was expected, since turbulence is not fully sustained at such low values of the friction Reynolds number, so that the dynamics of statistically coherent motion of fully turbulent flows remains close to that of transient turbulence and transition. However, by taking the spanwise-localized solution  $TW2 - 1$  as a new starting point, and continuing it to the statistically turbulent framework at sufficiently large friction number ( $Re_\tau \approx 380.03$ ), the statistically invariant motion considerably departs from the starting solution. This solution is characterized by large-scale and small-scale streaks reaching the wall, accompanied by rather small vortical structures further from the wall. These structures, as well as the main wavelengths and scaling of this statistically invariant solution are very close to those typical of the coherent motion in turbulent channel flows. In particular, the dominant wavelengths of the streamwise velocity premultiplied energy spectrum correspond to the typical spanwise size of large-scale structures (1.5 – 3.5 times the half channel height) and are characterized by a scaling  $y \approx 0.1 - 0.15\lambda_z$ , consistent with the attached eddy hypothesis. Whereas, spanwise lengths typical of the wall cycle and a scaling of  $y \approx 0.58\lambda_z$ ,  $y \approx \lambda_z$  are found in the spanwise and wall-normal spectra, respectively. Thus, the statistically steady solution presented here, constituted by large streaky structures and short vortical ones carrying all velocity components, is similar in shape and wavelengths to the self-sustaining structures of the attached eddy theory [11], although composed by large- and small-scale structures tied together in a non-trivial way. This statistically invariant solution may potentially represent one brick for the development of a low-order model of turbulence dynamics. It should be remarked that the comparison of the main wavelengths and scalings of this statistically invariant solution with those of the attached eddy has been limited to the spanwise direction, since the present solution has been obtained in a rather small streamwise domain. Future work will aim at continuing this or other solutions towards larger streamwise domains, as well as towards much higher friction Reynolds numbers. Moreover, new statistically invariant solutions might be obtained using as a starting point filtered snapshots of the turbulent flows, instead of continuing known invariant solutions of the Navier–Stokes equations. Finally, statistically periodic solutions can be recovered as well, providing relevant information about the temporal dynamics of the coherent part of the fluctuations in the considered statistical framework.

This might be a considerable step forward towards the development of reduced-order models of turbulent flows.

**Data accessibility.** Supporting data are accessible at the following link: <https://zenodo.org/record/5190924#.YRYiZsexXmg>.

**Authors' contributions.** E.P. carried out the computations and the data analysis under the indications of J.C.R., S.C. and P.D.P. M.F. helped in the development of the numerical code. S.C. conceived and designed the study, and drafted the manuscript. All authors read and approved the manuscript.

All authors gave final approval for publication and agreed to be held accountable for the work performed therein.

**Competing interests.** The authors declare that they have no competing interests.

**Funding.** This research was funded by MIUR grant no. PRIN 2017X7Z8S3\_002 LUBRI-SMOOTH. This work was granted access to the HPC resources of IDRIS under the allocation 2020-A0072A06362 and 2021-A0092A06362 made by GENCI.

## References

1. Barkley D, Song B, Mukund V, Lemoult G, Avila M, Hof B. 2015 The rise of fully turbulent flow. *Nature* **526**, 550–553. (doi:10.1038/nature15701)
2. Panton RL. 2001 Overview of the self-sustaining mechanisms of wall turbulence. *Prog. Aerosp. Sci.* **37**, 341–383. (doi:10.1016/S0376-0421(01)00009-4)
3. Kline SJ, Reynold WC, Schraub F, Rundstander P. 1967 The structure of turbulent boundary layer flows. *J. Fluid Mech.* **30**, 741–773. (doi:10.1017/S0022112067001740)
4. Landahl M. 1980 A note on an algebraic instability of inviscid parallel shear flows. *J. Fluid Mech.* **98**, 243–251. (doi:10.1017/S0022112080000122)
5. Hamilton JM, Kim J, Waleffe F. 1995 Regeneration mechanisms of near-wall turbulence structures. *J. Fluid Mech.* **287**, 317–348. (doi:10.1017/S0022112095000978)
6. Waleffe F. 1997 On a self-sustaining process in shear flows. *Phys. Fluids* **9**, 883–901. (doi:10.1063/1.869185)
7. Jiménez JJ, Pinelli A. 1999 The autonomous cycle of near-wall turbulence. *J. Fluid Mech.* **389**, 335–359. (doi:10.1017/S0022112099005066)
8. Hwang Y, Cossu C. 2010 Amplification of coherent streaks in the turbulent Couette flow: an input–output analysis at low Reynolds number. *J. Fluid Mech.* **643**, 333–348. (doi:10.1017/S0022112009992151)
9. Hwang Y, Cossu C. 2010 Self-sustained process at large scales in turbulent channel flow. *Phys. Rev. Lett.* **105**, 044505. (doi:10.1103/PhysRevLett.105.044505)
10. Hwang Y, Cossu C. 2011 Self-sustained processes in the logarithmic layer of turbulent channel flows. *Phys. Fluids (1994-present)* **23**, 061702. (doi:10.1063/1.3599157)
11. Hwang Y. 2015 Statistical structure of self-sustaining attached eddies in turbulent channel flow. *J. Fluid Mech.* **767**, 254–289. (doi:10.1017/jfm.2015.24)
12. Hwang J, Lee J, Sung HJ, Zaki TA. 2016 Inner–outer interactions of large-scale structures in turbulent channel flow. *J. Fluid Mech.* **790**, 128–157. (doi:10.1017/jfm.2016.3)
13. Cossu C, Hwang Y. 2017 Self-sustaining processes at all scales in wall-bounded turbulent shear flows. *Phil. Trans. R. Soc. A* **375**, 20160088. (doi:10.1098/rsta.2016.0088)
14. Kovasznay LSG, Kibens V, Blackwelder RF. 1970 Large-scale motion in the intermittent region of a turbulent boundary layer. *J. Fluid Mech.* **41**, 283–325. (doi:10.1017/S0022112070000629)
15. Komminaho J, Lundbladh A, Johansson AV. 1996 Very large structures in plane turbulent Couette flow. *J. Fluid Mech.* **320**, 259–285. (doi:10.1017/S0022112096007537)
16. Kim KC, Adrian RJ. 1999 Very large-scale motion in the outer layer. *Phys. Fluids* **11**, 417–422. (doi:10.1063/1.869889)
17. del Alamo JC, Jiménez J. 2003 Spectra of the very large anisotropic scales in turbulent channels. *Phys. Fluids* **15**, L41–L44. (doi:10.1063/1.1570830)
18. Hutchins N, Marusic I. 2007 Evidence of very long meandering features in the logarithmic region of turbulent boundary layers. *J. Fluid Mech.* **579**, 1–28. (doi:10.1017/S0022112006003946)
19. Townsend A. 1980 *The structure of turbulent shear flow*. Cambridge, UK: Cambridge University Press.



20. Nagata M. 1990 Three-dimensional finite-amplitude solutions in plane Couette flow: bifurcation from infinity. *J. Fluid Mech.* **217**, 519–527. (doi:10.1017/S0022112090000829)
21. Waleffe F. 1998 Three-dimensional states in plane shear flow. *Phys. Rev. Lett.* **81**, 4140–4143. (doi:10.1103/PhysRevLett.81.4140)
22. Kawahara G, Kida S. 2001 Periodic motion embedded in plane Couette turbulence: regeneration cycle and burst. *J. Fluid Mech.* **449**, 291–300. (doi:10.1017/S0022112001006243)
23. Waleffe F. 2001 Exact coherent structures in channel flow. *J. Fluid Mech.* **435**, 93–102. (doi:10.1017/S0022112001004189)
24. Faisst H, Eckhardt B. 2003 Travelling waves in pipe flow. *Phys. Rev. Lett.* **91**, 224502. (doi:10.1103/PhysRevLett.91.224502)
25. Hof B, van Doorne C, Westerweel J, Nieuwstadt F, Faisst H, Eckhardt B, Wedin H, Kerswell R, Waleffe F. 2004 Experimental observation of nonlinear traveling waves in turbulent pipe flow. *Science* **305**, 1594–1598. (doi:10.1126/science.1100393)
26. Wedin H, Kerswell R. 2004 Exact coherent structures in pipe flow: travelling wave solutions. *J. Fluid Mech.* **508**, 333–371. (doi:10.1017/S0022112004009346)
27. Eckhardt B, Schneider TM, Hof B, Westerweel J. 2007 Turbulence transition of pipe flow. *Annu. Rev. Fluid Mech.* **39**, 447–468. (doi:10.1146/annurev.fluid.39.050905.110308)
28. Duguet Y, Pringle CC, Kerswell RR. 2008 Relative periodic orbits in transitional pipe flow. *Phys. Fluids* **20**, 114102. (doi:10.1063/1.3009874)
29. Gibson JF, Halcrow J, Cvitanović P. 2009 Equilibrium and traveling-wave solutions of plane Couette flow. *J. Fluid Mech.* **638**, 243. (doi:10.1017/S0022112009990863)
30. Schneider TM, Gibson JF, Burke J. 2010 Snakes and ladders: localized solutions of plane Couette flow. *Phys. Rev. Lett.* **104**, 104501. (doi:10.1103/PhysRevLett.104.104501)
31. Willis AP, Cvitanović P, Avila M. 2013 Revealing the state space of turbulent pipe flow by symmetry reduction. *J. Fluid Mech.* **721**, 514–540. (doi:10.1017/jfm.2013.75)
32. Deguchi K, Hall P, Walton A. 2013 The emergence of localized vortex–wave interaction states in plane Couette flow. *J. Fluid Mech.* **721**, 58–85. (doi:10.1017/jfm.2013.27)
33. Gibson J, Brand E. 2014 Spanwise-localized solutions of planar shear flows. *J. Fluid Mech.* **745**, 25–61. (doi:10.1017/jfm.2014.89)
34. Zammert S, Eckhardt B. 2014 Streamwise and doubly-localised periodic orbits in plane Poiseuille flow. *J. Fluid Mech.* **761**, 348–359. (doi:10.1017/jfm.2014.633)
35. Park JS, Graham MD. 2015 Exact coherent states and connections to turbulent dynamics in minimal channel flow. *J. Fluid Mech.* **782**, 430–454. (doi:10.1017/jfm.2015.554)
36. Barnett J, Gurevich DR, Grigoriev RO. 2017 Streamwise localization of traveling wave solutions in channel flow. *Phys. Rev. E* **95**, 033124. (doi:10.1103/PhysRevE.95.033124)
37. Budanur N, Short KY, Farazmand M, Willis AP, Cvitanović P. 2017 Relative periodic orbits form the backbone of turbulent pipe flow. *J. Fluid Mech.* **833**, 274–301. (doi:10.1017/jfm.2017.699)
38. Hopf E. 1948 A mathematical example displaying features of turbulence. *Commun. Pure Appl. Math.* **1**, 303–322. (doi:10.1002/cpa.3160010401)
39. Farano M, Cherubini S, Robinet J-C, De Palma P, Schneider TM. 2019 Computing heteroclinic orbits using adjoint-based methods. *J. Fluid Mech.* **858**, R3. (doi:10.1017/jfm.2018.860)
40. Cvitanović P. 2013 Recurrent flows: the clockwork behind turbulence. *J. Fluid Mech.* **726**, 1–4. (doi:10.1017/jfm.2013.198)
41. Chandler GJ, Kerswell RR. 2013 Invariant recurrent solutions embedded in a turbulent two-dimensional Kolmogorov flow. *J. Fluid Mech.* **722**, 554–595. (doi:10.1017/jfm.2013.122)
42. Rawat S, Cossu C, Hwang Y, Rincon F. 2015 On the self-sustained nature of large-scale motions in turbulent Couette flow. *J. Fluid Mech.* **782**, 515–540. (doi:10.1017/jfm.2015.550)
43. Rawat S, Cossu C, Rincon F. 2016 Travelling-wave solutions bifurcating from relative periodic orbits in plane Poiseuille flow. *Comptes Rendus Mécanique* **344**, 448–455. (doi:10.1016/j.crme.2015.12.005)
44. Hwang Y, Willis AP, Cossu C. 2016 Invariant solutions of minimal large-scale structures in turbulent channel flow for  $re_\tau$  up to 1000. *J. Fluid Mech.* **802**, R1. (doi:10.1017/jfm.2016.470)
45. Azimi S, Cossu C, Schneider T. 2020 Self-sustained large-scale motions in the asymptotic suction boundary layer. (<http://arxiv.org/abs/2004.08862>)
46. Cimarelli A, De Angelis E, Jiménez J, Casciola CM. 2016 Cascades and wall-normal fluxes in turbulent channel flows. *J. Fluid Mech.* **796**, 417–436. (doi:10.1017/jfm.2016.275)



47. Cho M, Hwang Y, Choi H. 2018 Scale interactions and spectral energy transfer in turbulent channel flow. *J. Fluid Mech.* **854**, 474–504. (doi:10.1017/jfm.2018.643)
48. Doohan P, Willis AP, Hwang Y. 2021 Minimal multi-scale dynamics of near-wall turbulence. *J. Fluid Mech.* **913**, A8. (doi:10.1017/jfm.2020.1182)
49. Farano M, Cherubini S, Robinet J-C, De Palma P. 2017 Optimal bursts in turbulent channel flow. *J. Fluid Mech.* **817**, 35–60. (doi:10.1017/jfm.2017.107)
50. Farano M, Cherubini S, De Palma P, Robinet J-C. 2018 Nonlinear optimal large-scale structures in turbulent channel flow. *Eur. J. Mech. B Fluids* **72**, 74–86. (doi:10.1016/j.euromechflu.2018.04.016)
51. Eitel-Amor G, Örlü R, Schlatter P, Flores O. 2015 Hairpin vortices in turbulent boundary layers. *Phys. Fluids* **27**, 025108. (doi:10.1063/1.4907783)
52. Reynolds W, Tiederman W. 1967 Stability of turbulent channel flow, with application to Malkus's theory. *J. Fluid Mech.* **27**, 253–272. (doi:10.1017/S0022112067000308)
53. Cess R. 1958 *A survey of the literature on heat transfer in turbulent tube flow*. Report 8-0529-R24, Westinghouse Research.
54. Reynolds W, Hussain A. 1972 The mechanics of an organized wave in turbulent shear flow. part 3. Theoretical models and comparisons with experiments. *J. Fluid Mech.* **54**, 263–288. (doi:10.1017/S0022112072000679)
55. Del Alamo JC, Jimenez J. 2006 Linear energy amplification in turbulent channels. *J. Fluid Mech.* **559**, 205. (doi:10.1017/S0022112006000607)
56. Hwang Y. 2016 Mesolayer of attached eddies in turbulent channel flow. *Phys. Rev. Fluids* **1**, 064401. (doi:10.1103/PhysRevFluids.1.064401)
57. Pope SB. 2001 *Turbulent flows*. New York, NY: Cornell University.
58. Chen X, Hussain F, She Z-S. 2018 Quantifying wall turbulence via a symmetry approach. Part 2. Reynolds stresses. *J. Fluid Mech.* **850**, 401–438. (doi:10.1017/jfm.2018.405)
59. Kim J, Moin P, Moser R. 1987 Turbulence statistics in fully developed channel flow at low Reynolds number. *J. Fluid Mech.* **177**, 133–166. (doi:10.1017/S0022112087000892)
60. Moser RD, Kim J, Mansour NN. 1999 Direct numerical simulation of turbulent channel flow up to  $re \tau = 590$ . *Phys. Fluids* **11**, 943–945. (doi:10.1063/1.869966)
61. Pujals G, García-Villalba M, Cossu C, Depardon S. 2009 A note on optimal transient growth in turbulent channel flows. *Phys. Fluids (1994-present)* **21**, 015109. (doi:10.1063/1.3068760)
62. Gibson JF *et al.* In preparation. Channelflow 2.0.
63. Dean RB. 1978 Reynolds number dependence of skin friction and other bulk flow variables in two-dimensional rectangular duct flow. *J. Fluid Mech.* **100**, 215–223. (doi:10.1115/1.3448633)
64. de Giovanetti M, Sung HJ, Hwang Y. 2017 Streak instability in turbulent channel flow: the seeding mechanism of large-scale motions. *J. Fluid Mech.* **832**, 483–513. (doi:10.1017/jfm.2017.697)
65. Lee J, Lee J, Choi J, Sung H. 2014 Spatial organization of large- and very-large-scale motions in a turbulent channel flow. *J. Fluid Mech.* **749**, 818–840. (doi:10.1017/jfm.2014.249)